Materials Advances

ROYAL SOCIETY OF CHEMISTRY

COMMUNICATION

View Article Online
View Journal | View Issue

Cite this: *Mater. Adv.*, 2026, 7, 2003

Received 14th November 2025,
Accepted 26th December 2025

DOI: 10.1039/d5ma01330e

rsc.li/materials-advances

Influence of film formation kinetics on the dispersion of colloidal quantum dots in organic small molecule matrices

Rachel C. Kilbride, [ab] Michael P. Weir, [c] James Xiao, [d] Simon A. Dowland, [e] Jurjen F. Winkel, [e] John E. Anthony, [f] Akshay Rao, [d] Richard A. L. Jones, [g] Anthony J. Ryan [h] and Daniel T. W. Toolan *[i]

Improving the dispersion of colloidal quantum dots (QDs) within organic semiconductor (OSC) matrices remains critical for advancing hybrid nanocomposite optoelectronic technologies. This study investigates how film-deposition kinetics influence the morphology of TIPS-tetracene (TIPS-Tc):PbS QD blends, comparing spin-coating and blade coating for QDs ligated with either native oleic acid (OA) or a matched carboxylic acid functionalised tetracene analogue (TET-CA). Films spun-cast at low spin speeds form highly crystalline TIPS-Tc domains with highly aggregated QDs. Increased spin speed induces a deeper solvent quench, driving rapid TIPS-Tc nucleation while kinetically arresting QD diffusion, which improves QD dispersion within the crystalline matrix. TIPS-Tc:PbS-OA blends typically exhibit poor QD dispersibility due to poor matching between the OA ligands and the TIPS-Tc matrix. This work demonstrates that through employing high spin speeds QD dispersibilities may be significantly enhanced, even for PbS-OA, a significant step demonstrating that QD-OSC surface chemistries may not have to be fully matched to attain desired, well-dispersed morphologies. In contrast, blade-coating proceeds under slower solvent removal, resulting in weakly crystalline TIPS-Tc and extensive QD aggregation due to extended diffusion and delayed nucleation. These findings reveal the critical role of processing kinetics in directing OSC-QD self-assembly, essential for the optimisation of nanocomposite morphologies for next-generation optoelectronic devices.

1. Introduction

Organic semiconductor (OSC):quantum dot (QD) nanocomposites have emerged as promising materials for next-generation optoelectronic devices, combining the tunable optical and electronic properties of colloidal QDs with the excitonic functionality and solution processability of OSCs. These hybrid systems are of interest for a variety of applications, including photodetectors, photovoltaics and light-emitting diodes.[1–5] More recently, OSC:QD nanocomposites have gained attention as promising systems for singlet fission photon multiplication (SF-PM), a strategy to enhance the efficiency of silicon photovoltaics (Si-PV) beyond the Shockley–Queisser limit.[6–9] In SF-PM, high-energy photons are converted into multiple lower-energy photons through singlet fission in the OSC, which are subsequently absorbed by the QDs and re-emitted at lower energies that are better matched to the Si band gap. This process has the potential to raise the theoretical efficiency limit of Si-PV from ~33% to over 40%.[6,7,10,11] As in other OSC:QD systems, the performance of SF-PM nanocomposites is strongly governed by the nanoscale morphology of the blend film, where both the degree of QD dispersion and the local molecular organisation of the OSC matrix influence exciton transport, energy transfer, and SF-PM efficiency.[8,12,13] However, achieving a high degree of QD dispersion within a compatible OSC host remains a major challenge due to competing thermodynamic and kinetic factors during film formation, often resulting in a highly phase-separated film morphology.[14–16]

Our previous work has established a detailed framework for understanding the structural evolution of small-molecule OSC:QD blends, particularly in bis((triisopropylsilyl)ethynyl)tetracene (TIPS-tetracene, TIPS-Tc):PbS systems.[8,13,17,18] In these hybrid

[a] *Department of Physics, The University of Warwick, Coventry, CV4 7AL, UK*
[b] *XMaS, The UK X-ray Materials Science Facility, European Synchrotron Radiation Facility, F-38043, Grenoble, France*
[c] *School of Physics and Astronomy University of Nottingham, University Park, Nottingham, NG7 2RD, UK*
[d] *Cavendish Laboratory, University of Cambridge, J.J. Thomson Avenue, Cambridge, CB3 0HE, UK*
[e] *Cambridge Photon Technology, J.J. Thomson Avenue, Cambridge, CB3 0HE, UK*
[f] *University of Kentucky Centre for Applied Energy Research, 2582 Research Park Drive, Lexington, Kentucky, 40511, USA*
[g] *John Owens Building, The University of Manchester, Oxford Road, Manchester, M13 9PL, UK*
[h] *School of Mathematical and Physical Sciences, University of Sheffield, Brook Hill, Sheffield, S3 7HF, UK*
[i] *Department of Materials, University of Manchester, Engineering Building A, Booth Street East, Manchester, M13 9PL, UK. E-mail: daniel.toolan@manchester.ac.uk*

nanocomposites, the surface chemistry of the QDs plays a central role in directing self-assembly and determining film morphology. Singlet fission in TIPS-Tc and triplet transfer to PbS QDs functionalised with 6,11-bis((triisopropylsilyl)ethynyl)-tetracene-2-carboxylic acid (TET-CA) ligands (PbS–TET-CA) has been reported widely,[19–22] with solid-state SF-PM systems now achievable.[8,23] Here, the TET-CA ligand, derived from a singlet fission-capable OSC, provides a dual advantage: (i) improved energetic and electronic coupling that enhances exciton transfer between the OSC and QDs, and (ii) increased chemical compatibility with the TIPS-Tc host, resulting in markedly better QD dispersion compared with native long-chain oleic acid (OA) ligands. Improved QD dispersion enhances exciton transfer and SF-PM efficiency, demonstrating the central role of QD surface chemistry in determining nanocomposite function. Beyond ligand design, the introduction of mixed small-molecule OSC matrices has been shown to improve QD dispersibility, demonstrating that subtle changes in host composition can substantially influence the balance between OSC crystallisation and QD dispersion.[18]

Complementary scattering and microscopy investigations have also revealed how film-formation kinetics govern the final composite structure.[12,13,17,24] *In situ* studies of TIPS-Tc:PbS blends prepared by blade-coating identified two distinct self-assembly routes for PbS-TET-CA QDs depending on the composition of the host OSC (TIPS-Tc or 9,10-Bis[(triisopropylsilyl)ethynyl]anthracene (TIPS-Ac)).[17] For TIPS-Tc, QD aggregation acts to nucleate the crystallisation of the OSC and the subsequent crystallisation of the OSC acts to expel the QD nanoparticle inclusions. In contrast, for TIPS-Ac, crystallisation of the OSC occurs spontaneously and subsequently expels the QD inclusions.[17] Spatially resolved photophysical mapping later confirmed that variations in local morphology directly influence triplet generation and SF-PM efficiency, with regions rich in QD aggregates exhibiting reduced performance.[12] The studies highlight the crucial role of OSC–ligand miscibility and drying kinetics in influencing self-assembly and the final, functional OSC:QD nanocomposite morphology.

Despite this progress, the relative influence of thermodynamic and kinetic factors during film formation and the impact of film processing parameters remains poorly understood. In this work, we systematically compare the morphology of TIPS-Tc in blends with PbS QDs functionalised with OA and TET-CA ligands with films prepared by two common film preparation routes: spin-coating and blade-coating. Spin-coating induces rapid solvent evaporation and a deep kinetic quench, often resulting in non-equilibrium morphologies,[25–28] whilst blade-coating, a scalable deposition method, involves directional and relatively slow solvent removal, achieving morphologies close to thermodynamic equilibrium.[29] A comparative investigation of these techniques provides a route to decouple the effects of ligand chemistry from the influence of deposition kinetics on QD dispersion and OSC crystallisation. By varying the spin speed to tune the solvent-quench rate, we demonstrate that faster film formation significantly enhances QD dispersibility within the TIPS-Tc matrix. High-speed spin-coating produces improved QD dispersion compared to blade-coating, and even the PbS-OA system, which is typically prone to aggregation, achieves relatively good QD dispersibility under rapid quench conditions. These results show that processing kinetics can override equilibrium ligand effects, providing new mechanistic insight into QD–OSC self-assembly, crucial to optimising the performance of SF-PM and related optoelectronic technologies.

2. Results and discussion

PbS QDs were synthesised *via* a previously reported method,[30] with the as-synthesised native oleic acid (OA) ligands exchanged with a matched tetracene carboxylic acid derivative (TET-CA) to obtain OA- and TET-CA-ligated PbS QDs (PbS-OA and PbS-TET-CA respectively) as illustrated in Fig. 1a. Previous small angle X-ray and neutron scattering (SAXS/SANS) of the as-synthesised PbS-OA QDs in toluene confirm the nanoparticles have PbS cores measuring 22 Å in radius with a lognormal polydispersity of 0.14.[8,13]

First, the nanomorphology of TIPS-Tc:PbS-OA and TIPS-Tc:PbS-TET-CA blends prepared *via* spin-coating at a range of spin speeds (500, 1500, and 6000 rpm) is discussed. During spin-coating, the solution is rapidly spread by centrifugal force as the substrate rotates at high angular velocity, often resulting in rapid solvent evaporation and a deep quench into the solid state. As a result, film-drying behaviour can be tuned by adjusting parameters such as spin speed, solution concentration, and solution temperature. Alongside intrinsic material properties, these parameters dictate solvent evaporation and crystallisation dynamics, which in turn determine the degree of QD aggregation and the final film morphology.

To characterise film morphology, grazing incidence small- and wide-angle X-ray scattering (GISAXS and GIWAXS) were performed on composite TIPS-Tc:PbS-OA and TIPS-Tc:PbS-TET-CA blend films prepared *via* spin-coating at 500, 1500, and 6000 rpm. Two-dimensional (2D) GIWAXS and GISAXS patterns are shown in Fig. 1b and c respectively, with corresponding azimuthally integrated one-dimensional (1D) intensity profiles shown in Fig. 1d. GIWAXS (wide angle region, q = 0.4–1.3 Å^{-1}) was used to probe the influence of spin speed on the packing and crystallinity of the TIPS-Tc host while GISAXS (small angle region, q = 0.05–0.4 Å^{-1}) provides insights into QD ordering and packing (where $q = 4\pi\sin\theta/\lambda$, θ is half the scattering angle, and λ is the X-ray wavelength). The 2D GIWAXS patterns display several high-intensity diffraction peaks, confirming that TIPS-Tc is highly crystalline in all spin-coated films. However, comparison of the corresponding 1D intensity profiles reveals that increasing spin speed leads to broader and lower-intensity TIPS-Tc scattering features, indicating a reduction in crystallinity for both the PbS-OA and PbS-TET-CA systems (Fig. 1b).

Inspection of the GISAXS region reveals that spin-speed and QD surface chemistry strongly influence QD ordering, giving rise to significantly different small angle scattering in the q range 0.05–0.4 Å^{-1} (Fig. 1c). The obtained scattering patterns

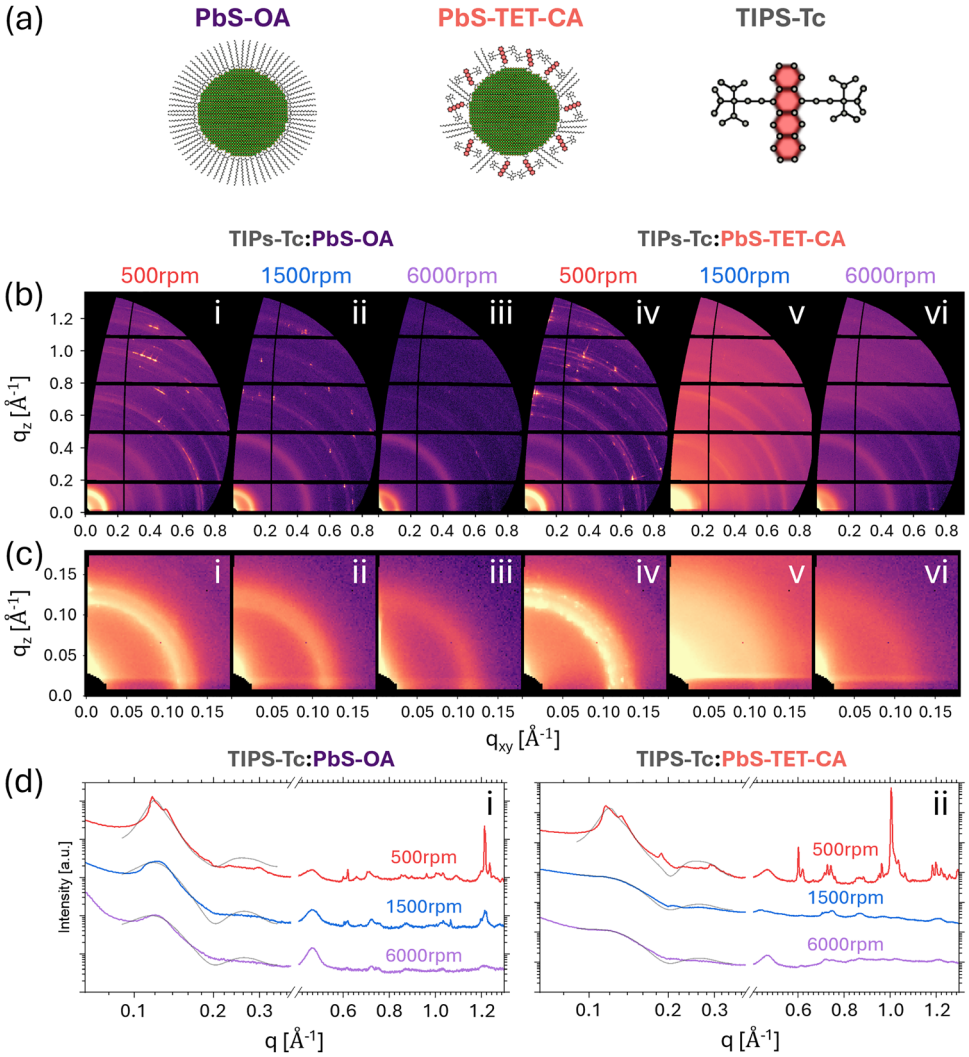

Fig. 1 (a) Illustration of PbS QDs possessing either oleic acid (PbS-OA) or tetracene carboxylic acid (PbS-TET-CA) ligands and small molecule host, TIPS-tetracene (TIPS-Tc). (b) and (c) 2D GIXS data of (i, ii, iii) TIPS-Tc:PbS-OA and (iv, v, vi) TIPS-Tc:PbS-TET-CA OSC:QD blends deposited *via* spin-coating at speeds of 500 rpm, 1500 rpm and 6000 rpm. (d) Corresponding azimuthally integrated 1D intensity profiles of (i) TIPS-Tc:PbS-OA and (ii) TIPS-Tc:PbS-TET-CA prepared *via* spin-coating and the associated fits to the GISAXS region (grey lines) using an FCC paracrystal model. The 1D data have been multiplied by an arbitrary coefficient to be shifted along the intensity axis for clarity. Note the peak at $q \sim 0.45$ Å^{-1} is a background peak from the Kapton window.

exhibit a wide range of QD arrangements, ranging from (i) well-ordered/packed QDs with a pronounced structure factor peak at $q \sim 0.12$ Å^{-1}, consistent with face-centred cubic (FCC) superlattice features, to (ii) more dispersed, randomly arranged QDs with scattering closely resembling the form factor of non-interacting spherical particles. At low spin speeds (500 rpm), a distinct structure factor peak is visible at $q \sim 0.12$ Å^{-1}, consistent with a highly aggregated QD arrangement. As spin speed is increased, the intensity of this structure factor peak decreases for both QD-ligand systems, suggesting an increase in dispersibility of QDs within the TIPS-Tc matrices. The effect is more pronounced for TIPS-Tc:PbS-TET-CA systems, indicating that the improved chemical compatibility of the TET-CA ligand enhances the dispersion of PbS-TET-CA compared to native PbS-OA QDs and is consistent with previous studies.[8,13] However, it is striking that PbS-OA systems, which are typically prone to aggregation,[8,13,31] demonstrate relatively good QD dispersibility under rapid quench conditions (*i.e.* fast spin speeds). This observation suggests that further optimisation of spin-coating parameters could enhance PbS-OA dispersibility, offering a potential route to control self-assembly in systems that typically display unfavourable blend morphologies.

The dispersibility of PbS-OA and PbS-TET-CA QDs in TIPS-Tc is characterised more quantitatively through fitting the low q region of the azimuthally integrated 1D intensity profiles (Fig. 1d). Here, the QD scattering data has been fitted using an FCC colloidal paracrystal model (grey lines), with full fit parameters displayed in Table S1 (Further information regarding the FCC paracrystal model is provided in the Supplementary Information, Section S1.1). This model has been

employed previously to describe QD ordering in blends comprising small molecule polyacenes and QDs.[8,17,18] As shown in simulated 1D profiles (Supplementary Information, Section S1.2), the disorder parameter obtained from the FCC paracrystal model provides a direct measure for quantifying the QD dispersibility within the host TIPS-Tc matrix, where low disorder parameters correspond to a highly ordered FCC arrangement of QDs (*e.g.* highly aggregated) and high disorder parameters correspond to weakly ordered QD arrangements (were a value of 1.0 is equivalent to randomly dispersed QDs that could be described by a scattering model of spheres with hard-sphere interactions).

It should be noted that at low spin-speeds the FCC paracrystal model begins to fit the data less-well then in instances where the QDs are relatively well dispersed at higher spin-speeds, however, such fits do effectively capture the most significant scattering features. Discrepancies between the fits likely arises from the presence of diffraction spots in the 2D scattering data that indicate the formation of relatively large, highly ordered, randomly ordered FCC QD crystallites. In addition, to these diffraction spots, more typical isotropic

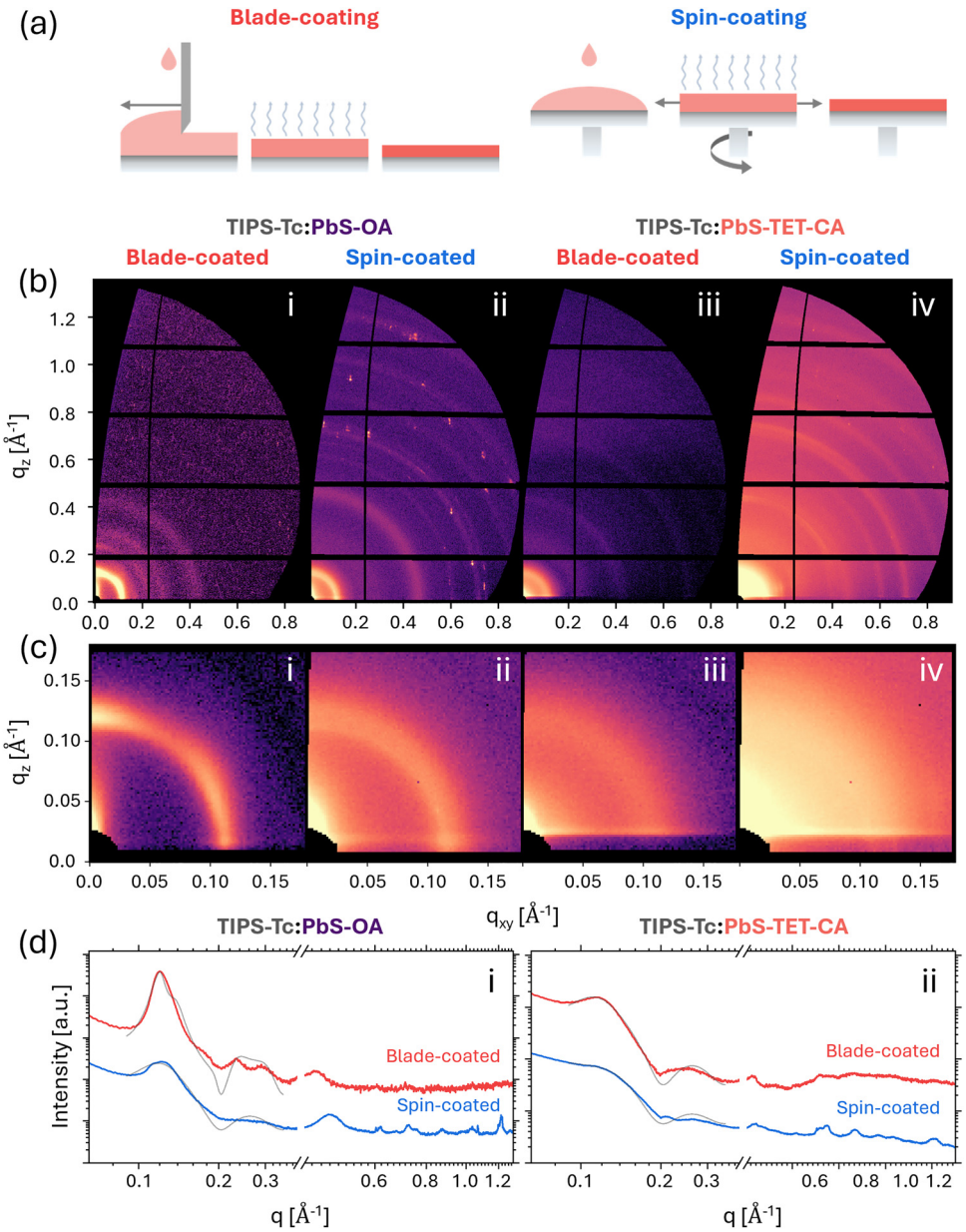

Fig. 2 (a) Schematic of blade-coating and spin-coating film deposition techniques. 2D (b) GIWAXS and (c) GISAXS data of (i, ii) TIPS-Tc:PbS-OA and (iii, iv) TIPS-Tc:PbS-TET-CA OSC:QD blends deposited *via* blade-coating and spin-coating at 1500 rpm. (d) Corresponding azimuthally integrated 1D intensity profiles of (i) TIPS-Tc:PbS-OA and (ii) TIPS-Tc:PbS-TET-CA prepared *via* blade-coating (red line) and spin-coating (blue line), and the associated fits to the GISAXS data (grey lines) using an FCC paracrystal model. The 1D data have been multiplied by an arbitrary coefficient to be shifted along the intensity axis for clarity. Note the peak at $q \sim 0.45$ Å^{-1} is a background peak from the Kapton window.

scattering features commensurate with disorder QD aggregates are visible. We do not attempt to fully fit and deconvolute scattering contributions between these two QD morphologies here as these are the worst case scenarios for intended applications of OSC:QD blend systems and serve as an exemplar of how given appropriate drying conditions the OSC matrix material will aim to exclude QD impurities and thus generate such poorly mixed morphologies.

Fitting the low q, QD scattering region with the FCC paracrystal model shows that low spin-speeds yield low disorder parameters in the range 0.15–0.17, with higher spin speeds increasing the disorder parameter to ~0.3 and ~0.45 for blends comprising PbS-OA and PbS-TET-CA QDs respectively (Fig. 1d and Table S1). This trend is consistent with reduced QD aggregation at higher spin speeds and improved chemical compatibility of the TET-CA ligand.

In addition to the disorder parameter, the FCC paracrystal model yields a corresponding lattice constant that represents the average centre-to-centre spacing between QDs within locally ordered domains. For PbS QDs with a core radius of ~22 Å and typical ligand shell lengths of ~10–20 Å, a close-packed arrangement would be expected to give a lattice constant in the range of ~60–80 Å, depending on the degree of ligand interdigitation. The lattice constants extracted here fall within this range for films spin-coated at low spin speeds (500 rpm) but decrease for films spin-coated at higher spin speeds due to increasing QD disorder (Table S1). This apparent contraction does not indicate physical compression of the QD lattice but rather reflects a reduction in the coherence length of the QD assembly and a transition from ordered superlattices to more disordered, locally correlated distributions. In these highly dispersed films, the lattice constant becomes a nominal descriptor of short-range QD spacing rather than a true crystallographic periodicity. Taken together, the correlated trends in disorder parameter and lattice constant indicate that enhanced ligand compatibility and faster solvent removal during spin-coating at high spin-speeds disrupt long-range QD ordering, yielding weaker interparticle correlations and improved QD dispersion within the TIPS-Tc matrix.

Consistent with the spin-speed-dependent changes in TIPS-Tc scattering, cross-polarised optical microscopy (Fig. S4) shows that the morphologies of films coated at low spin-speeds (500 rpm) comprise large crystal grains with large spherulitic features, with the TIPS-Tc:PbS-OA blend exhibiting banded type spherulites, indicative of TIPS-Tc crystallisation occurring under diffusion limited conditions. The TIPS-Tc:PbS-TET-CA blend morphology does not contain the same banded type spherulites, likely indicating that TIPS-Tc crystallisation occurred earlier on in the film formation process. For TIPS-Tc:PbS-OA/PbS-TET-CA coated at 1500 and 6000 rpm the cross polarised optical microscopy images shown the presence of large aspherical crystalline features embedded within a fine matrix of much smaller crystallites. Such morphologies have been observed previously,[12] and the absence of a Maltese cross in the large crystalline features indicates a multi-grain, misoriented texture, consistent with QD incorporation perturbing nucleation and crystallisation to yield a more stochastic, likely multi-step crystallisation process.

Building on the observation that higher spin-coating speeds suppresses QD aggregation, we extended our study to include blade-coating: a scalable film deposition technique compatible with large-area manufacturing. While both spin-coating and blade-coating rely on solvent evaporation to drive film formation, the drying kinetics differ substantially. During blade-coating, a liquid meniscus is translated across the substrate at a controlled coating speed, typically resulting in slower solvent removal and providing more time for molecular self-assembly and phase separation (Fig. 2a). In addition to intrinsic material and solution properties, the film-drying behaviour in blade-coated films can be tuned by adjusting the blade height and

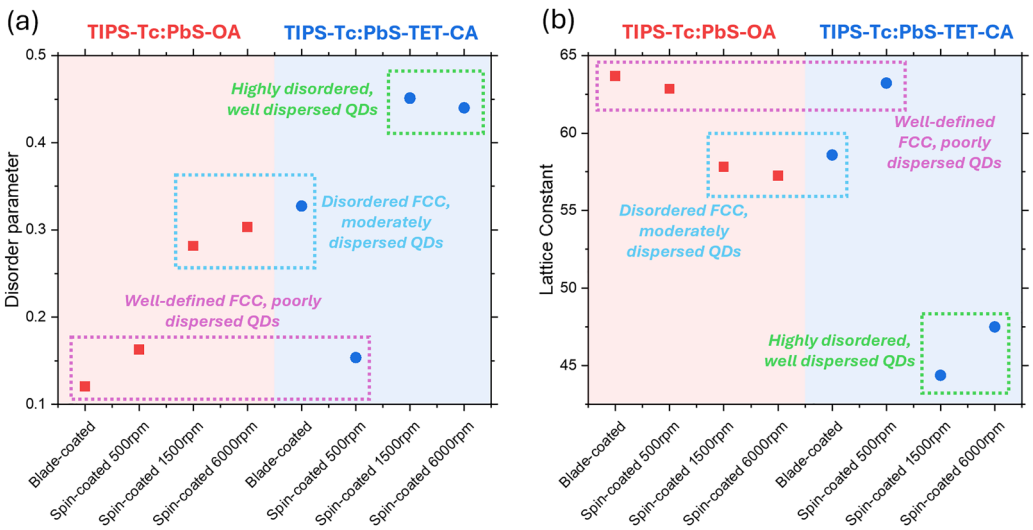

Fig. 3 QD (a) disorder parameters and (b) lattice constants derived from the FCC paracrystal model fit to the GISAXS data shown in Fig. 1d and 2d for TIPS-Tc:PbS-OA and TIPS-Tc:PbS-TET-CA OSC:QD blends deposited *via* blade-coating and spin-coating at various speeds.

coating speed,[32] allowing OSC:QD self-assembly to be optimised.

To evaluate the effects of deposition technique on film morphology, GIWAXS and GISAXS measurements were performed on TIPS-Tc:PbS-OA and TIPS-Tc:PbS-TET-CA blend films prepared *via* blade-coating and spin-coating at 1500 rpm. Representative 2D GIWAXS and GISAXS patterns are shown in Fig. 2b and c, with corresponding azimuthally integrated 1D intensity profiles shown in Fig. 2d. Consistent with observations for spin-coated films, the TET-CA ligand enhances chemical compatibility with the TIPS-Tc host, improving QD dispersion in blade-coated films relative to native PbS-OA. Quantitatively, this is reflected in the FCC paracrystal fit parameters which give disorder parameters of $\sim$0.12 and $\sim$0.33 and lattice constants of $\sim$64 Å and $\sim$59 Å for PbS-OA and PbS-TET-CA respectively (Table S1 and Fig. 2d). Compared with spin-coated films, the QD dispersibility of blade-coated films are similar to films prepared at lower spin-speeds (500 rpm).

Focusing on QD dispersibility, all systems studied in this work can be grouped into three categories, as illustrated in Fig. 3a:

(i) Well-defined FCC, poorly dispersed QDs: blade-coated PbS-OA films and those spin-coated at low spin speeds (500 rpm) fall into this category. These films exhibit low disorder parameters ($<$0.2) and large lattice constants ($>$60 Å), indicative of ordered but aggregated QD domains.

(ii) Disordered FCC, moderately dispersed QDs: this category includes blade-coated PbS-TET-CA films and PbS-OA films spin-coated at higher speeds. These systems show intermediate disorder parameters (0.2–0.4) and lattice constants of 50–60 Å, reflecting partial disruption of long-range QD ordering and improved dispersion.

(iii) Highly disordered, well-dispersed QDs: PbS-TET-CA films spin-coated at high speeds exhibit disorder parameters $>$0.4 and lattice constants $<$50 Å, consistent with strong disruption of FCC order and high QD dispersibility throughout the TIPS-Tc matrix.

In contrast to spin-coated films, which exhibit highly crystalline TIPS-Tc matrices, the GIWAXS patterns of blade-coated films display broad, low-intensity rings indicative of significantly reduced crystallinity (Fig. 2b). The concurrent suppression of TIPS-Tc ordering and enhanced QD aggregation in blade-coated films relative to their spin-coated counterparts suggests that the two deposition methods promote subtly different self-assembly pathways that occur during film formation. We hypothesise that the observed morphological differences between spin-coated and blade coated TIPS-Tc:QD blends likely arise from the interplay between solvent evaporation dynamics, supersaturation kinetics, and phase segregation behaviour during film deposition.[33–38] During spin-coating, we speculate that rapid solvent removal drives a deep supersaturation of TIPS-Tc, promoting high nucleation densities and fast crystallisation while the residual solvent still permits limited molecular mobility. This short-lived window favours the formation of highly crystalline TIPS-Tc domains and likely kinetically traps QDs before extensive exclusion of QDs from growing TIPS-Tc crystalline domains is able to occur.[12,13,17,18] At higher spin speeds, the increased evaporation rate enhances such kinetic trapping, improving QD dispersibility through limiting molecular reorganisation, but also leads to reduced TIPS-Tc crystallinity. In addition, it should be noted that undercooling due to solvent removal during spin-coating has been reported previously,[39] which will increase nucleation rates and promotes the formation of a large number of small TIPS-Tc crystals.

In contrast, slower solvent evaporation during blade coating yields lower supersaturation and minimal undercooling, which lowers nucleation rates while extending the time for molecular reorganisation before vitrification.[28] Under these conditions, QDs likely aggregate independently of TIPS-Tc nucleation and crystal growth, most plausibly *via* liquid–liquid phase separation processes.[40,41] Because undercooling is weak and nucleation density is low, crystallisation cannot keep pace with solvent loss, and the TIPS-Tc vitrifies. Consequently, the blade-coated films possess morphologies possessing both poor QD dispersibility and poor TIPS-Tc crystallinity, where it may be envisaged that lower crystallinity would improve QD dispersibility.

3. Conclusions

In this work, we demonstrate how simply increasing spin-speeds can be employed to improve QD dispersibility within crystalline TIPS-Tc films, even when the surface chemistry of the QD ligands is not matched to the surface chemistry of the TIPS-Tc matrix, as is the case for PbS-OA. Higher spin-speeds promote the formation of smaller TIPS-Tc crystallites in the film, combined with faster drying and vitrification kinetics that limit the formation of either random QD packed aggregates or ordered FCC packed QD superlattice type structures. Consistent with previous works,[8,13] matching the ligand chemistry of the QD to that of the TIPS-Tc matrix ultimately produces the best QD dispersibility, however, it is striking that control of processing parameters can yield similar dispersibilities, illustrating the importance of both kinetic and thermodynamic effects in determining the morphologies of such hybrid OSC:QD blend films.

When the same TIPS-Tc:PbS-OA/PbS-TET-CA blends were blade coated rather then spun-cast we observe both a decrease in the dispersibility of the QDs and in the degree of crystallinity of the TIPS-Tc. This result is counter to what may be predicted where crystallisation drives the exclusion of QD impurities from the growing TIPS-Tc crystallites, as we have previously reported.[12,13,17] This result leads us to hypothesise that it is likely that a further liquid–liquid phase separation mechanism may occur generating QD aggregates, independent of TIPS-Tc crystallisation and occurs for blade coated films when in regimes of both low nucleation density and slower crystallisation kinetics.

These results demonstrate how translating from spin-coating to more scalable coating approaches such as blade coating is non-trivial if films possessing similar morphologies are desired and are illustrated in Fig. 4. This work paves the way

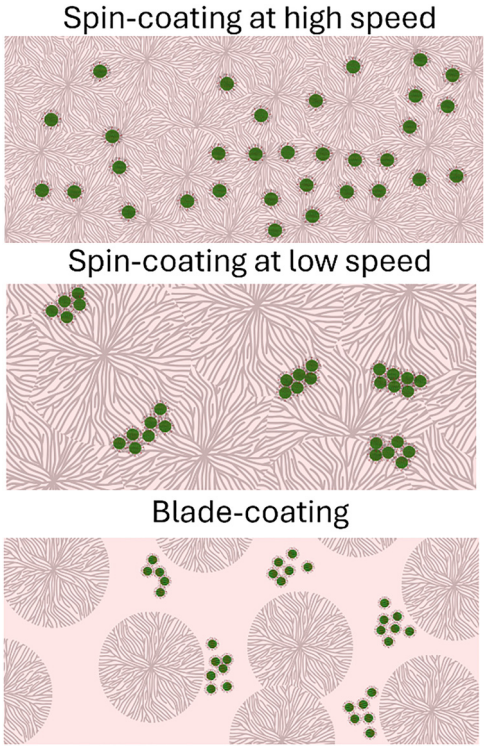

Fig. 4 Illustration of the different OSC:QD morphologies formed in TIPS-Tc:PbS-OA and TIPS-Tc:PbS-TET-CA blend films when processed by spin-coating at high and low spin speeds and by blade-coating.

for further exploration of how the effects of both temperature, evaporation rate and consequently concentration,[42] could be employed to control the highly intricate self-assembly processes in OSC:QD films.

4. Experimental methods

Materials

5,12-Bis((triisopropylsilyl)ethynyl)tetracene (TIPS-Tc) and 6,11-bis((triisopropylsilyl)ethynyl)tetracene-2-carboxylic acid (TET-CA) were synthesised as described previously.[43,44]

Synthesis of lead sulphide-oleic acid (PbS-OA) QDs

A master batch of oleic acid-capped PbS QDs was synthesised by the method of Hines & Scholes.[30] Lead oxide (PbO, 99.999%) was purchased from Alfa Aesar. Ethanol and 1-butanol (Hi-Dry anhydrous) were purchased from Romil. All other chemicals were purchased from Sigma-Aldrich. All materials were used as received without further purification. Lead oxide (1.25 g, 5.6 mmol), oleic acid (OA, 90%, 4 mL, 12.6 mmol) and 1-octadecene (ODE, 90%, 25 mL, 78 mmol) were placed in a 3-necked round-bottomed flask and degassed under vacuum ($<10^{-2}$ mbar) at 110 °C for 2 hours with stirring, forming a colorless solution. In a nitrogen glovebox, a syringe was prepared containing ODE (13.9 mL, 43 mmol) and hexamethyldisilathiane (TMS2S, 95%, 592 μL, 2.8 mmol). The flask was put under nitrogen flow and the syringe contents rapidly injected into the flask at 110 °C and allowed to cool. Upon cooling to 60 °C, the reaction mixture was transferred to an argon glovebox. The as formed nanocrystals were precipitated with ethanol/butanol and centrifuged at 12 000 g. The QDs were then suspended with hexane and precipitated again with ethanol. The purified QDs were suspended in toluene at 100 mg mL^{-1} for storage.

Exchange of PbS-OA to PbS-TET-CA

Ligand exchange of synthesised OA-capped PbS QDs with TIPS-tetracenecarboxylic acid was performed as follows. TIPS-tetracene carboxylic acid was dissolved in toluene (20 mg mL^{-1}) and added to PbS QDs in toluene (50 mg mL^{-1}). The mixture was stirred at room temperature overnight before precipitation with acetone and centrifugation at 12 000 g. The exchanged nanocrystals were resuspended in toluene, and the purification was repeated, with final resuspension in toluene to form a reddish-black solution.

Film preparation

Silicon substrates were cleaned by sonication for 10 mins in a DI water and detergent (Decon90) mixture, followed by acetone and then isopropanol before being blown dry with compressed N_2.

A TIPS-Tc stock solution was prepared in toluene (200 mg mL^{-1}) and heated to 50 °C for 1 h and vortex-mixed prior to use. The TIPS-Tc:PbS casting solution was prepared by mixing the TIPS-Tc stock solution by volume with PbS-OA or PbS-Tet-CA stock solutions to prepare solutions containing a total TIPS-Tc content of 100 mg mL^{-1} and total QD content of 10 mg mL^{-1}.

Preparation of spin-coated samples: 50 μL of casting solution was deposited on silicon substrates and spun-cast at speeds of 500, 1500 or 6000 rpm for 2 min. All samples were prepared in a nitrogen glovebox.

Preparation of blade coated samples: 100 μL of casting solution was coated onto silicon substrates using a RK (K101) Coater at room temperature in a nitrogen glovebox. The speed selected was ''speed 8'' which is approximately 8 mm s^{-1}.

Spun cast and blade coated samples were stored under nitrogen prior to X-ray measurements.

Grazing incidence X-ray scattering

GIXS measurements were performed on a Xeuss 2.0 SAXS/WAXS laboratory beamline (Xenocs, Grenoble, France) equipped with an liquid gallium MetalJet X-ray source (Excillum Kista, Sweden), wavelength of characteristic radiation λ = 1.34 Å. The same configuration was used in each experiment. Scattering patterns were recorded on a vertically-offset Pilatus 1M detector (Dectris) with a sample to detector distance of 550 mm, calibrated using a silver behenate standard to achieve a q-range of 0.065–1.3 $Å^{-1}$. Two-dimensional images were recorded with exposure times of 900 s. Alignment was performed on silicon substrates *via* three iterative height (z) and rocking curve (Ω) scans, with the final grazing incidence angle set to $\Omega = 0.3°$. Detector images were corrected, reshaped and reduced using python code which relies on pyFAI and pygix libraries.[45] Azimuthally integrated q-dependent 1D intensity

profiles were performed across the full azimuthal angle (χ) and q ranges using a mask to remove contributions from erroneous "hot pixels", the substrate horizon and the reflected beam. Reduced 1D intensity profiles were fitted in SasView software in the q range 0.09 $Å^{-1}$ < q < 0.35 $Å^{-1}$ using root square scattering intensity data, |sqrt(I)| weighting and the Nelder-Mead Simplex algorithm.[46]

Polarised optical microscopy

The polorised optical microscopy images were collected using a Nikon ME600 optical microscope mounted on an isolation table and fitted with a Pixelink PL-A742 machine vision camera and using a 10×, magnification objective (Nikon). A calibration graticule was used to calibrate the lengthscale for the optical images. An analyser and polarizer were placed in the optical path and the polarizer rotated to enhance the contrast. The program ImageJ was used to add a scale bar to the optical images.

Conflicts of interest

The authors declare the following competing financial interest(s): AR is a founder of Cambridge Photon Technology, a company commercialising advanced solar cell technologies, of which SD, JW is an employee. The other authors declare no competing non-financial interests.

Data availability

The scattering data supporting this article have been included at DOI: https://doi.org/10.48420/31026385 and as part of the supplementary information (SI) and the 1D Scattering data was fitted using SASView https://www.sasview.org/. Supplementary information is available. See DOI: https://doi.org/10.1039/d5ma01330e.

Acknowledgements

The authors acknowledge funding through the Engineering and Physical Sciences Research Council (UK) *via* grant EP/V055127/1 and EP/Y031962/1. This work benefited from the use of the SasView application, originally developed under NSF award DMR-0520547. SasView also contains coding developed with funding from the European Union's Horizon 2020 Research and Innovation Program under the SINE2020 project, grant agreement no. 654000. The authors are grateful for funding from the EPSRC to purchase (EP/M028437/1) and upgrade (EP/V034804/1) the Xeuss 2.0 SAXS/WAXS laboratory beamline at the Soft Matter Analytical Laboratory of the University of Sheffield.

References

1 A. J. Moulé, L. Chang, C. Thambidurai, R. Vidu and P. Stroeve, Hybrid solar cells: basic principles and the role of ligands, *J. Mater. Chem.*, 2012, **22**, 2351–2368.
2 J. Niederhausen, K. A. Mazzio and R. W. MacQueen, Inorganic–organic interfaces in hybrid solar cells, *Electron. Struct.*, 2021, **3**, 33002.
3 M. Zorn, *et al.*, Quantum Dot−Block Copolymer Hybrids with Improved Properties and Their Application to Quantum Dot Light-Emitting Devices, *ACS Nano*, 2009, **3**, 1063–1068.
4 W. G. Lawrence, S. Thacker, S. Palamakumbura, K. J. Riley and V. V. Nagarkar, Quantum Dot-Organic Polymer Composite Materials for Radiation Detection and Imaging, *IEEE Trans. Nucl. Sci.*, 2012, **59**, 215–221.
5 G. N. Ankah, *et al.*, PbS quantum dot based hybrid-organic photodetectors for X-ray sensing, *Org. Electron.*, 2016, **33**, 201–206.
6 M. H. Futscher, A. Rao and B. Ehrler, The Potential of Singlet Fission Photon Multipliers as an Alternative to Silicon-Based Tandem Solar Cells, *ACS Energy Lett.*, 2018, **3**, 2587–2592.
7 A. Rao and R. H. Friend, Harnessing singlet exciton fission to break the Shockley–Queisser limit, *Nat. Rev. Mater.*, 2017, **2**, 17063.
8 V. Gray, *et al.*, Ligand-Directed Self-Assembly of Organic-Semiconductor/Quantum-Dot Blend Films Enables Efficient Triplet Exciton-Photon Conversion, *J. Am. Chem. Soc.*, 2024, **146**, 7763–7770.
9 W. Shockley and H. J. Queisser, Detailed Balance Limit of Efficiency of p-n Junction Solar Cells, *J. Appl. Phys.*, 2004, **32**, 510.
10 J. Lee, *et al.*, Singlet Exciton Fission Photovoltaics, *Acc. Chem. Res.*, 2013, **46**, 1300–1311.
11 M. J. Y. Tayebjee, A. Rao and T. W. Schmidt, All-optical augmentation of solar cells using a combination of up- and downconversion, *J. Photonics Energy*, 2018, **8**, 22007.
12 D. T. W. Toolan, *et al.*, Linking microscale morphologies to localised performance in singlet fission quantum dot photon multiplier thin films, *J. Mater. Chem. C*, 2022, **10**, 11192–11198.
13 D. T. W. Toolan, *et al.*, Insights into the Structure and Self-Assembly of Organic-Semiconductor/Quantum-Dot Blends, *Adv. Funct. Mater.*, 2022, **32**, 2109252.
14 M. L. Huggins, Solutions of Long Chain Compounds, *J. Chem. Phys.*, 1941, **9**, 440.
15 P. J. Flory, Thermodynamics of High Polymer Solutions, *J. Chem. Phys.*, 1941, **9**, 660.
16 L. X. Reynolds, *et al.*, Charge photogeneration in hybrid solar cells: A comparison between quantum dots and in situ grown CdS, *Nanoscale*, 2012, **4**, 1561–1564.
17 D. T. W. Toolan, *et al.*, Insights into the kinetics and self-assembly order of small-molecule organic semiconductor/quantum dot blends during blade coating, *Nanoscale Horiz.*, 2023, **8**, 1090–1097.
18 D. T. W. Toolan, *et al.*, Mixed Small-Molecule Matrices Improve Nanoparticle Dispersibility in Organic Semiconductor-Nanoparticle Films, *Langmuir*, 2023, **39**, 4799–4808.
19 J. R. Allardice, *et al.*, Engineering Molecular Ligand Shells on Quantum Dots for Quantitative Harvesting of Triplet

Excitons Generated by Singlet Fission, *J. Am. Chem. Soc.*, 2019, **141**, 12907–12915.
20 V. Gray, *et al.*, Direct vs Delayed Triplet Energy Transfer from Organic Semiconductors to Quantum Dots and Implications for Luminescent Harvesting of Triplet Excitons, *ACS Nano*, 2020, **14**, 4224–4234.
21 N. J. L. K. Davis, *et al.*, Singlet Fission and Triplet Transfer to PbS Quantum Dots in TIPS-Tetracene Carboxylic Acid Ligands, *J. Phys. Chem. Lett.*, 2018, **9**, 1454–1460.
22 V. Gray, *et al.*, Triplet transfer from PbS quantum dots to tetracene ligands: is faster always better?, *J. Mater. Chem. C*, 2022, **10**, 16321–16329.
23 T. K. Baikie, *et al.*, Singlet Fission Luminescent Solar Concentrators, *Nano Lett.*, 2025, **25**, 16204–16211.
24 D. T. W. Toolan, *et al.*, Controlling the structures of organic semiconductor–quantum dot nanocomposites through ligand shell chemistry, *Soft Matter*, 2020, **16**, 7970–7981.
25 D. T. W. Toolan, S. Fujii, S. J. Ebbens, Y. Nakamura and J. R. Howse, On the mechanisms of colloidal self-assembly during spin-coating, *Soft Matter*, 2014, **10**, 8804–8812.
26 D. T. W. Toolan and J. R. Howse, Development of in situ studies of spin coated polymer films, *J. Mater. Chem. C*, 2013, **1**, 603–616.
27 D. T. W. Toolan, *et al.*, Direct observation of morphological development during the spin-coating of polystyrene–poly(methyl methacrylate) polymer blends, *J. Polym. Sci., Part B: Polym. Phys.*, 2013, **51**, 875–881.
28 E. U. Haq, *et al.*, Real time laser interference microscopy for bar-spread polystyrene/poly(methyl methacrylate) blends, *J. Polym. Sci., Part B: Polym. Phys.*, 2014, **52**, 985–992.
29 C. M. Stafford, K. E. Roskov, H. I. I. I. Epps Thomas and M. J. Fasolka, Generating thickness gradients of thin polymer films via flow coating, *Rev. Sci. Instrum.*, 2006, **77**, 23908.
30 M. A. Hines and G. D. Scholes, Colloidal PbS Nanocrystals with Size-Tunable Near-Infrared Emission: Observation of Post-Synthesis Self-Narrowing of the Particle Size Distribution, *Adv. Mater.*, 2003, **15**, 1844–1849.
31 F. Xu, *et al.*, Impact of Different Surface Ligands on the Optical Properties of PbS Quantum Dot Solids, *Materials*, 2015, **8**, 1858–1870.
32 Z. Peng, *et al.*, Real-Time Probing and Unraveling the Morphology Formation of Blade-Coated Ternary Nonfullerene Organic Photovoltaics with In Situ X-Ray Scattering, *Adv. Funct. Mater.*, 2023, **33**, 2213248.
33 K. Foroutani, *et al.*, Conducting Polymer-Based Coatings and Thin Films: A Review on Film Processing and Deposition Techniques, *Polym. Rev.*, 2025, **65**, 1057–1100.
34 C. Schaefer, J. J. Michels and P. van der Schoot, Structuring of Thin-Film Polymer Mixtures upon Solvent Evaporation, *Macromolecules*, 2016, **49**, 6858–6870.
35 J. J. van Franeker, *et al.*, Controlling the Dominant Length Scale of Liquid–Liquid Phase Separation in Spin-coated Organic Semiconductor Films, *Adv. Funct. Mater.*, 2015, **25**, 855–863.
36 S. Eickelmann and H. Riegler, Rupture of ultrathin solution films on planar solid substrates induced by solute crystallization, *J. Colloid Interface Sci.*, 2018, **528**, 63–69.
37 A. Mandal, *et al.*, Diffusion-Induced Thickness Thinning of Spin-Coated Films in Crystalline Grain Boundaries: A Process of Amorphization, *Adv. Mater. Interfaces*, 2023, **10**, 2202293.
38 D. T. W. Toolan, N. Pullan, M. J. Harvey, P. D. Topham and J. R. Howse, In Situ Studies of Phase Separation and Crystallization Directed by Marangoni Instabilities During Spin-Coating, *Adv. Mater.*, 2013, **25**, 7033–7037.
39 D. P. Birnie III, B. J. J. Zelinski and D. L. Perry, Infrared observation of evaporative cooling during spin-coating processes, *Opt. Eng.*, 1995, **34**, 1782–1788.
40 S. Xu, H. Zhang, B. Qiao and Y. Wang, Review of Liquid–Liquid Phase Separation in Crystallization: From Fundamentals to Application, *Cryst. Growth Des.*, 2021, **21**, 7306–7325.
41 I. Zhang, C. P. Royall, M. A. Faers and P. Bartlett, Phase separation dynamics in colloid–polymer mixtures: the effect of interaction range, *Soft Matter*, 2013, **9**, 2076–2084.
42 H. Mejri, *et al.*, Gas-assisted blade-coating of organic semiconductors: molecular assembly{,} device fabrication and complex thin-film structuring, *Nanoscale*, 2022, **14**, 17743–17753.
43 S. A. Odom, S. R. Parkin and J. E. Anthony, Tetracene Derivatives as Potential Red Emitters for Organic LEDs, *Org. Lett.*, 2003, **5**, 4245–4248.
44 S. Garakyaraghi, C. Mongin, D. B. Granger, J. E. Anthony and F. N. Castellano, Delayed Molecular Triplet Generation from Energized Lead Sulfide Quantum Dots, *J. Phys. Chem. Lett.*, 2017, **8**, 1458–1463.
45 G. Ashiotis, *et al.*, The fast azimuthal integration Python library: pyFAI, *J. Appl. Crystallogr.*, 2015, **48**, 510–519.
46 SasView - Small Angle Scattering Analysis, https://www.sasview.org/.